Trans. Phenom. Nano Micro Scales, 6(2): 79-87, Summer and Autumn 2018
DOI:10.22111/tpnms.2018.20403.1128

ORIGINAL RESEARCH PAPER

Slip flow in porous micro-tubes under local thermal non-equilibrium conditions

Abdollah Goli, Iman Zahmatkesh*

Department of Mechanical Engineering, Mashhad Branch, Islamic Azad University, Mashhad, Iran

Received 30 December 2016; revised 19 May 2017; accepted 28May 2017; available online 3 July 2018

ABSTRACT: In the present work, forced convection heat transfer of slip flow in porous micro-tubes with local thermal non-equilibrium between the gas and the solid matrix is investigated numerically. For this purpose, the flow is considered hydrodynamically developed but thermally developing. The Darcy-Brinkman-Forchheimer model in conjunction with separate energy equations for the gas and the solid matrix is used to describe the flow and heat transfer in the porous media. Moreover, both velocity slip and temperature jump are applied to the fluid at the wall. Simulation results are presented in terms of velocity field, distributions of the fluid and solid temperatures, the local Nusselt number, and the thermal entry length. The results indicate heat transfer improvement as a result of increase in the Peclet/Biot number. Increase in the Knudsen number or the modified conductivity ratio, however, diminishes the heat transfer rate. Although the choice of the Darcy/Forchheimer number may change the computational results, trends are not similar in the developing and the developed regions of the flow.

KEYWORDS: *Forced convection; fully developed flow; micro-tube; porous media; slip flow*

INTRODUCTION

Current developments in production techniques of micro-electro-mechanical systems (MEMS) have drawn attentions to describe flow and heat transfer in micro-channels. Gas flows through micro-channels experience rarefied consequences. The criterion for the flow rarefaction is the Knudsen number which is defined as the ratio of the molecular mean-free-path to the characteristic length of the problem. Schaaf and Chambre [1] have classified dilute gas flows in terms of the Knudsen number. Afterwards, Gad-el-Hak [2] has offered a modified classification as: (1) the continuum regime ($Kn \leq 0.001$), (2) the slip regime ($0.001 < Kn \leq 0.1$), (3) the transition regime ($0.1 < Kn \leq 10$), and (4) the free molecular regime ($10 < Kn$).

In the slip regime, the flow equations remain accurate. But, the conditions of no-slip and no-temperature jump are no longer valid. Thereby, velocity slip and temperature jump boundary conditions must be applied to the fluid at the walls [3,4].

Slip flows in micro-channels with different cross-sections have been analyzed extensively in the past. Nevertheless, those in channels occupied by porous media have received less attention due to the additional parameters involved in their description. Haddad and his colleagues have presented numerical solutions for hydrodynamically developed but thermally developing slip flows in porous micro-ducts [5] andporous micro-tubes [6]. The Darcy-Brinkman-Forchheimer model in conjunct-ion with the local thermal equilibrium (LTE) assumption between the gas and the solid matrix was used during these investigations. Further, they analyzed local thermal non-equilibrium (LTNE) effects in porous micro-ducts [7], adopting separate energy equations for the gas and the solid matrix.

Thereafter, Shokouhmand et al. [8] employed a Knudsen-dependent relation for the fluid viscosity and extended the work of Haddad et al. [5] to a wide range of the Knudsen number.

Some analytic solutions for the slip flows in porous micro-channels have also been accomplished. The proposed solutions are limited to the Darcy-Brinkman model. They are also restricted to cases with fully developed flow and thermal fields.

Neild and Kuzentsov [9] have presented analytic solutions for slip flows in porous micro-ducts and mirco-tubes under LTE conditions.

The assumption of LTE has also been used in the investigation of Hooman [10] that presented closed form solutions for slip flows in porous micro-channels with rectangular cross-sections.

Analytic solutions for flow and thermal fields in porous micro-ducts under LTNE conditions have been proposed by Mahmoudi [11] and Buonomo et al. [12]. Recently, Buonomo et al. [13] have improved their analytic solutions to include viscous dissipation. Exact solutions for flow and thermal fields in porous micro-tubes under LTE conditions have been offered by Wang et al. [14]. More recently, Torabi and Peterson [15] have analyzed the first law and the second law of thermodynamics in porous micro-channels with thick walls under magnetic field.

*Corresponding Author Email:*Zahmatkesh5310@mshdiau.ac.ir*
Tel.: +989155109399; Note. This manuscript was submitted on December30, 2016; approved on May 28, 2017; published online July 3, 2018.

Nomenclature

Bi	Biot Number
c_f	coefficient in the Forchheimer term
c_P	constant pressure specific heat (J/kg.K)
Da	Darcy number
H	local heat transfer coefficient (W/m^2.K)
h_{sf}	solid to fluid heat transfer coefficient (W/m^2.K)
K	thermal conductivity (W/m.K)
K	permeability of the porous media (m^2)
Kn	Knudsen number
K_R	modified conductivity ratio
L	length of the micro-tube (m)
L_{th}	thermal entry length (m)
Nu	local Nusselt number
p	pressure (Pa)
Pe	Peclet number
Pr	Prandtl number
r	radial coordinate (m)
r_0	radius of the micro-tube (m)
R	dimensionless radial coordinate
Re_D^*	modified Reynolds number
T	temperature (K)
U	axial velocity (m/s)
u_0	reference axial velocity (m/s)
U	dimensionless axial velocity
z	axial coordinate (m)
Z	dimensionless axial coordinate
	Subscripts
f	fluid
m	mean value
s	solid
w	wall
	Greek Symbols
α	thermal diffusivity (m^2/s)
γ	specific heat ratio
Γ	Forchheimer number
λ	mean-free-path (m)
ϕ	porosity
μ	dynamic viscosity (kg/m.s)
ρ_f	fluid density
σ	tangential-momentum-accommodation coefficient
σ_T	thermal-accommodation coefficient
θ	dimensionless temperature

Although previous investigations on the slip flows in porous micro-channels are important, many parts of the flow and heat transfer need to be resolved, especially when the thermal field is developing or LTNE prevails. In the present paper, attention is focused to analyze these effects simultaneously. For this purpose, forced convection heat transfer in porous micro-tubes is simulated numerically. Computations are undertaken for distinct cases with different values of the Knudsen number, the Darcy number, the Peclet number, the Forchheimer number, the Biot number, and the modified conductivity ratio. Results are presented in terms of velocity field, distributions of the fluid and solid temperatures, the local Nusselt number, and the thermal entry length.

MATHEMATICAL FORMULATION

Consider forced convection of steady laminar Newtonian flow in a porous micro-tube as shown in Figure 1.

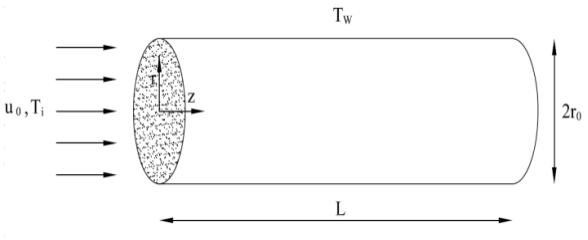

Fig. 1. Configuration of the porous micro-tube

The flow is hydrodynamically developed but thermally developing. So, the velocity component in the *r*-direction is zero while the velocity component in the *z*-direction is only a function of *r*. The fluid temperature is also a function of *r* and *z*.

The slip flow regime is simulated and discussed here. Thereby, the Darcy-Brinkman-Forchheimer model in conjunction with velocity slip and temperature jump boundary conditions is applicable.

The Mach number of the gas flow in the porous micro-tube is small compared to unity.

As a result, compressibility effects are negligible and we limit our attention to the rarefied ones. Thermophysical properties of the gas are taken constant. The contributions of the buoyancy force, the radiation heat transfer, and the viscous dissipation are also ignored.

Additionally, the fluid is not assumed to be in LTE with the solid matrix. So, we use separate energy equations for the gas and the solid matrix.

Moreover, the porous media is taken isotropic, rigid, and homogeneous.

With these assumptions, the governing equations in the cylindrical coordinate system become [16]:

Momentum equation

$$0 = -\frac{dp}{dz} + \frac{\mu_f}{\phi}\left(\frac{1}{r}\frac{\partial u}{\partial r} + \frac{\partial^2 u}{\partial r^2}\right) - \frac{\mu_f}{K}u - \frac{c_f \rho_f}{\sqrt{K}}u^2 \qquad (1)$$

Fluid-phase energy equation

$$\rho_f c_P u \frac{\partial T_f}{\partial z} = \phi k_f \left(\frac{1}{r}\frac{\partial T_f}{\partial r} + \frac{\partial^2 T_f}{\partial r^2}\right) + h\left(T_s - T_f\right) \qquad (2)$$

Solid-phase energy equation

$$0 = (1-\phi)k_s\left(\frac{1}{r}\frac{\partial T_s}{\partial r}+\frac{\partial^2 T_s}{\partial r^2}\right) - h\left(T_s - T_f\right) \tag{3}$$

With the introduction of the following dimensionless parameters:

$$\begin{aligned} &R=\frac{r}{r_0},\quad Z=\frac{z}{r_0},\quad U=\frac{u}{u_0}, u_0=\frac{\phi r_0^2}{-\mu\, dp/dz}\\ &Re_D^*=\frac{2\rho_f u_0 r_0}{\mu\phi}, Da=\frac{K}{\phi r_0^2}, Kn=\frac{\lambda}{r_0}, Pr=\frac{\mu_f}{\alpha_f\rho_f}\\ &\theta=\tfrac{T-T_i}{T_w-T_i},\quad \theta_m=\tfrac{T_m-T_i}{T_w-T_i},\quad Bi=\tfrac{h_{sf}r_0^2}{\phi k_f},\\ &K_R=\frac{\phi k_f}{(1-\phi)k_s},\quad \Gamma=\frac{-\rho_f c_f \phi^2 r_0^4\, dp/dz}{\mu^2\sqrt{K}} \end{aligned} \tag{4}$$

the dimensionless governing equations can be expressed as:

Momentum equation

$$1+\frac{\partial^2 U}{\partial R^2}+\frac{1}{R}\frac{\partial U}{\partial R}-\frac{1}{Da}U-\Gamma U^2=0 \tag{5}$$

Fluid-phase energy equation

$$U\frac{\partial\theta_f}{\partial Z}=\frac{1}{Pe}\left[\frac{1}{R}\frac{\partial\theta_f}{\partial R}+\frac{\partial^2\theta_f}{\partial R^2}+Bi\left(\theta_s-\theta_f\right)\right] \tag{6}$$

Solid-phase energy equation

$$0=\frac{1}{R}\frac{\partial\theta_s}{\partial R}+\frac{\partial^2\theta_s}{\partial R^2}-Bi\,K_R\left(\theta_s-\theta_f\right) \tag{7}$$

Here, Pe is the Peclet number ($Pe = Re_D^*\mathrm{Pr}$).
Equations (5-7) are subjected to the following boundary conditions:

Symmetry

$$\frac{\partial U}{\partial R}(Z,0)=\frac{\partial\theta_f}{\partial R}(Z,0)=\frac{\partial\theta_s}{\partial R}(Z,0)=0 \tag{8}$$

Inlet

$$\theta_f(0,R)=0, \theta_s(0,R)=0 \tag{9}$$

Outlet

$$\frac{\partial\theta_f}{\partial Z}(L/r_0,R)=0, \frac{\partial\theta_s}{\partial Z}(L/r_0,R)=0 \tag{10}$$

At the tube wall, the solid temperature is equal to that of the wall (i.e., $\theta_s(Z,R=1)=1$). For the fluid velocity and temperature, however, the following velocity slip and temperature jump boundary conditions are applied [17]:

Fluid temperature at the wall

$$\theta_f(Z,1)=1-\frac{2-\sigma_T}{\sigma_T}\left[\frac{2\gamma}{\gamma+1}\right]\frac{Kn}{Pr}\frac{\partial\theta_f}{\partial R}\bigg|_{R=1} \tag{11}$$

Fluid velocity at the wall

$$U(Z,1)=-\frac{2-\sigma}{\sigma}Kn\left(\frac{\partial U}{\partial R}\right)_{R=1} \tag{12}$$

Here, the values of the tangential-momentum-accommodation coefficient (σ) and the thermal-accommodation coefficient (σ_T) are taken equal to 0.7.

NUMERICAL SOLUTION

In this study, the finite difference method is used to solve the governing equations. The set of algebraic equations obtained from the finite difference approximation are three-diagonal.

This allows us to employ the Thomas algorithm for their solution. Since the momentum equation can be decoupled from the energy equations, it is solved firstly. Using the obtained velocity field, the energy equations for the gas and solid matrix are then solved simultaneously. As velocity and thermal fields become available from a converged solution, the local Nusselt number is obtained from the following relation:

$$Nu=\frac{2hr_0}{\phi k_f}=\frac{2}{1-\theta_m}\left(\frac{\partial\theta_f}{\partial R}+\frac{1}{K_R}\frac{\partial\theta_s}{\partial R}\right)_{R=1} \tag{13}$$

With

$$\theta_m=\frac{\int_0^1 U\theta R\, dR}{\int_0^1 UR\, dR} \tag{14}$$

To obtain a grid suitable for the range of governing parameters studied here, a grid independence test isperformed. It is found that refinement of the grid from 100×200 to 150×300 may not change the Nusselt numbers more than 1% for a case with $Kn=0.1, Pe=35, Da=1$, and $\Gamma=1$. Further investigations also verify the suitability of such a grid under other circumstances. So, a 100×200 grid is selected for the current computations.

RESULTS AND DISCUSSION

To establish the accuracy of the current numerical solution, two validation studies are undertaken here. Firstly,

we compare our simulation results with the exact solution of Haddad et al. [6] in terms of velocity distribution in Figure 2. Secondly, the local Nusselt numbers are compared with the numerical results of Haddad et al. [6] under LTE conditions in Figure 3.

Comparison of the results in both of the figures indicates good agreement. This provides confidence to the employed solution procedure for further studies. So, in the foregoing section, it is used to analyze the velocity field, the distributions of the fluid and solid temperatures, the local Nusselt number, and the thermal entry length. for the slip flow in porous micro-tubes. The consequences of the Knudsen number, the Peclet number, the Darcy number, the Forchheimer number, the Biot number, and the modified conductivity ratio on the heat transfer performance are also discussed.

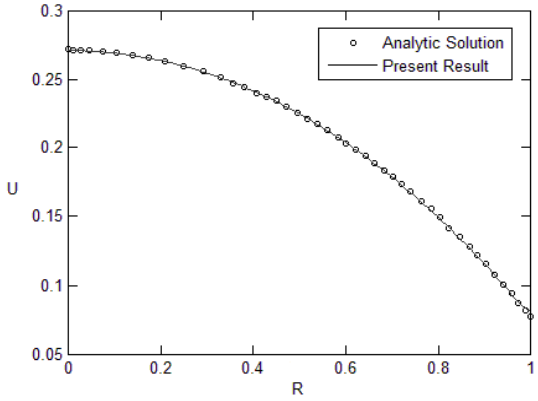

Fig. 2. The obtained velocity distribution compared with that of the exact solution of Haddad et al. [6] ($Kn = 0.1, Da = 1, \Gamma = 0$)

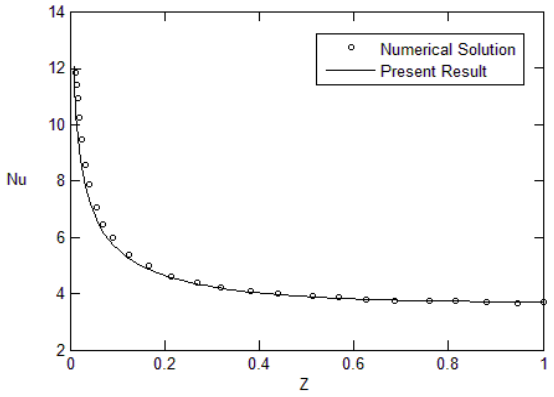

Fig. 3. The obtained distribution of the local Nusselt number compared with that of the numerical results of Haddad et al. [6] ($Kn = 0.01, Pe = 35, Da = 1, \Gamma = 0.1$)

Effect of the Knudsen number on the radial distribution of the axial velocity is analyzed in Figure 4 for the whole range of the gas rarefaction in the slip flow regime. The figure demonstrates that with increase in the Knudsen number, both the velocity magnitudes and the velocity slip increase, in such a way that the rise in the velocity slip is higher. This indicates that as the gas rarefaction becomes more pronounced, the retarding effect of the wall diminishes that increases the flow rate through the micro-tube.

The figure also demonstrates that rarefied effects are more significant at the larger values of the Knudsen numbers (i.e., $0.01 \leq Kn \leq 0.1$).

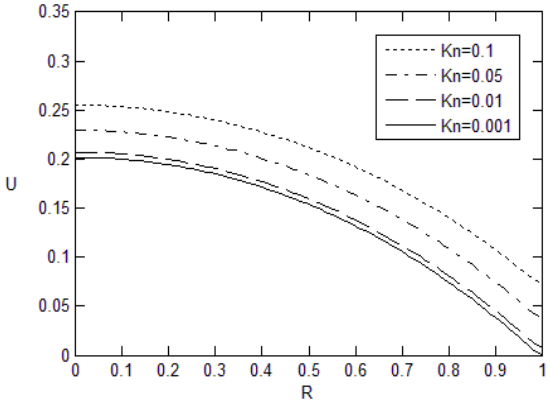

Fig. 4. Effect of the Knudsen number on the distribution of velocity ($Da = 1, \Gamma = 1$)

Figures 5 and 6 illustrate the consequences of the gas rarefaction on the distributions of the fluid and solid temperatures at different sections through the micro-tube. Notice in Figure 5 that with increase in the Knudsen number, the fluid temperature shifts down.

Physical reasoning for this behavior is the fact that the rise in the Knudsen number leads to more flow through the micro-tube followed by the need to warm greater amount of the fluid. Additionally, as the flow becomes more rarefied, the wall temperature jump increases (see $\theta_f(Z, 1)$), which in turn reduces the heat exchange between the wall and the adjacent fluid.

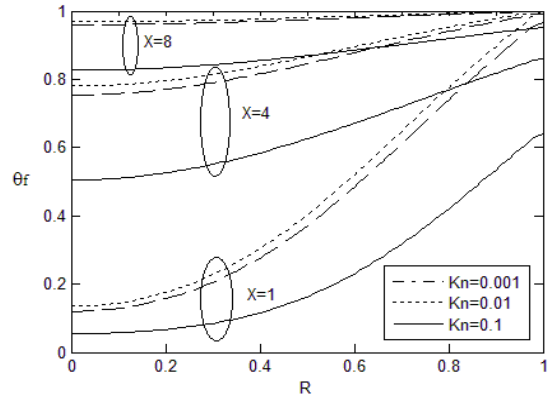

Fig. 5. Effect of the Knudsen number on the distribution of the fluid temperature at different sections through the micro-tube ($Pe = 100$, $Da = 1, \Gamma = 10, Bi = 1, K_R = 1$)

As a result of the fluid-solid interactions, it is not surprising to see similar trend in the dependency of the

solid temperature to the Knudsen number in Figure 6, i.e., the solid temperature decreases with increase in the Knudsen number. Notice, however, that thermal contact of the solid matrix with the tube wall removes the temperature jump there. So, one observes higher temperatures in the solid, as compared to the fluid.

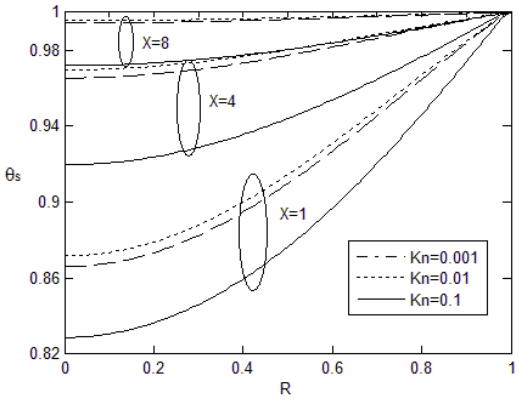

Fig. 6. Effect of the Knudsen number on the distribution of the solid temperature at different sections through the micro-tube
$(Pe = 100, Da = 1, \Gamma = 10, Bi = 1, K_R = 1)$

Figures 7 and 8 show the effects of the Darcy number and the Forchheimer number on the fluid temperature at different sections through the micro-tube. Notice the lower temperature rise in the higher values of the Darcy number or the lower values of the Forchheimer number. This lower temperature rise occurs as a result of the increased gas flow rate through the tube, followed by need to warm greater amount of the fluid. The figures also demonstrate that variations of the wall temperature jump as a result of changes in the Darcy/Forchheimer number are not so substantial.

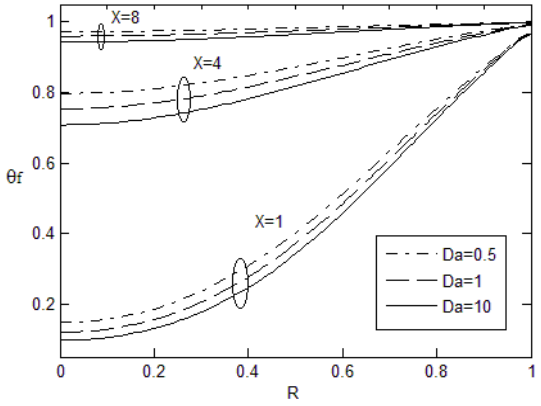

Fig. 7. Effect of the Darcy number on the distribution ofthe fluid temperatureat different sections through the micro-tube
$(Kn = 0.01, Pe = 100, \Gamma = 10, Bi = 1, K_R = 1)$

Closer scrutiny of Figure 8 indicates that the results of $\Gamma = 0.1$ and $\Gamma = 1$ are almost identical. This allows one to conclude that the inertial resistance of the medium is effective just in sufficiently large values of Γ.

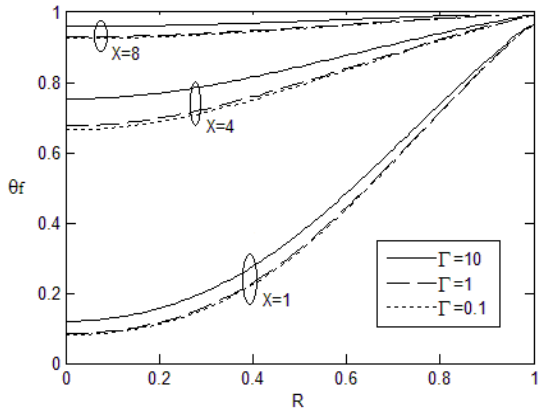

Fig. 8. Effect of the Forchheimer number on the distribution of the fluid temperature at different sections through the micro-tube
$(Kn = 0.01, Pe = 100, Da = 1, Bi = 1, K_R = 1)$

Next, the consequences of the Darcy number and the Forchheimer number on the solid temperature are depicted in Figures 9 and 10, respectively. Obviously, the trends are similar to the fluid temperature. This is expected due to their interactions.

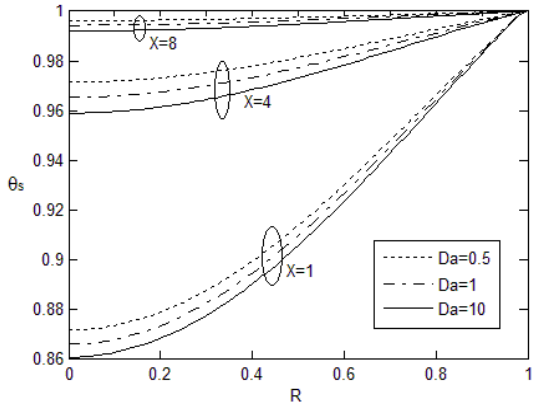

Fig. 9. Effect of the Darcy number on the distribution of the solid temperatureat different sections through the micro-tube
$(Kn = 0.01, Pe = 100, \Gamma = 10, Bi = 1, K_R = 1)$

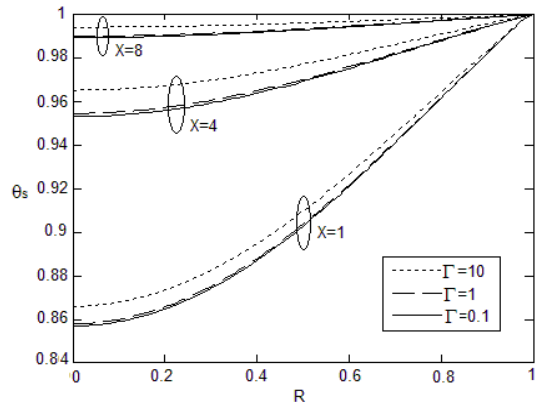

Fig. 10. Effect of the Forchheimer number on the distribution of the solid temperature at different sections through the micro-tube
$(Kn = 0.01, Pe = 100, Da = 1, Bi = 1, K_R = 1)$

Figures 11 and 12 plot the temperature distributions in the fluid and the solid matrix for different values of the Peclet number. Although the Peclet number is not so influential in the temperature distributions at $X = 8$, notice its dominant role, especially in the fluid temperature at the starting section of the tube. It is obvious that the higher Peclets produce the lower temperature rise both in the fluid and the solid matrix. This is again attributed to the greater gas flow rate that prevails at higher Peclet numbers.

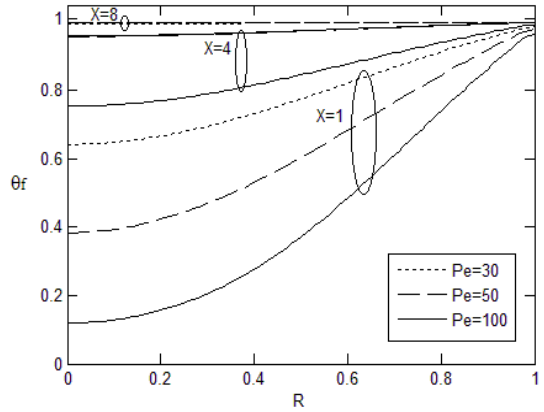

Fig. 11. Effect of the Peclet number on the distribution of the fluid temperature at different sections through the micro-tube ($Kn = 0.01, Da = 1, \Gamma = 10, Bi = 1, K_R = 1$)

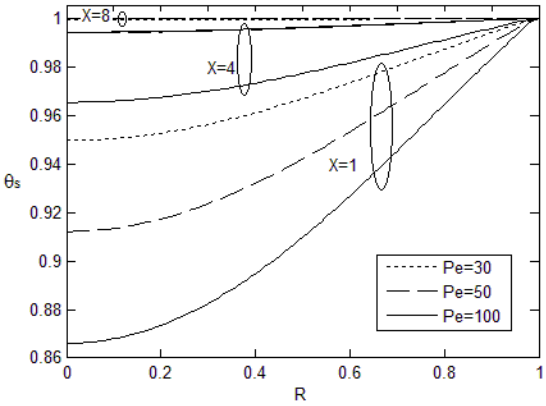

Fig. 12. Effect of the Peclet number on the distribution of the solid temperature at different sections through the micro-tube ($Kn = 0.01, Da = 1, \Gamma = 10, Bi = 1, K_R = 1$)

The distribution of the local Nusselt number through the micro-tube for different values of the Knudsen number is provided in Figure 13.

Notice that as we proceed along the tube, the Nusselt number decreases considerably. This is expected due to the growth of the thermal boundary layer. With further movement along the tube, however, the flow becomes thermally developed. So, the Nusselt number tends to a constant value. Although the gas rarefaction is not so effective at the lower values of the Knudsen numbers (i.e., $0.001 \leq Kn \leq 0.01$), notice that as the Knudsen number increases from 0.01 to 0.1, the Nusselt number diminishes. This is attributed to the increased temperature jump at the wall that avoids the near wall fluid feeling the real temperature of the wall. From a molecular point of view, an increment in the Knudsen number deteriorates the number of collisions between the gas molecules and the wall and thereby, energy flux of the reflected molecules decreases.

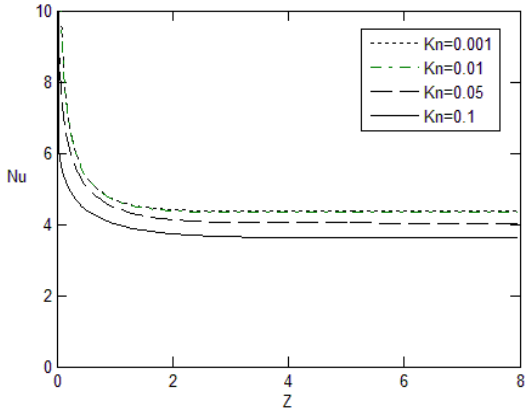

Fig. 13. Effect of the Knudsen number on the distribution of the local Nusselt number through the micro-tube ($Pe = 100, Da = 1, \Gamma = 10, Bi = 1, K_R = 1$)

It is noteworthy that the increased gas flow velocity as a result of the enhanced rarefaction tends to elevate the Nusselt number, but this effect is not dominant here. Closer scrutiny of the figure indicates that with increase in the Knudsen number, the flow needs more distance to become thermally developed.

The influence of the Darcy number on the distribution of the local Nusselt number is outlined in Figure 14. Although the results of $0.5 \leq Da \leq 10$ are almost identical, notice that this parameter does not produce similar consequences in the developing and the developed regions of the tube.

This occurs since with increase in the Darcy number (i.e., decrease in the frictional resistance of the medium), both velocity slip and temperature jump increase at the wall. Here, the increased velocity slip tends to increase the Nusselt number while the increased temperature jump produces an opposite effect.

When the gas flow is developing, the increased velocity slip is dominant causing heat transfer improvement as a result of increase in the Darcy number. Conversely, in the thermally developed region, the increased temperature jump overcomes the effect of the increased velocity slip. This makes the Nusselt number diminishes with increase in the Darcy number.

The dependencies of the wall velocity slip and temperature jump to the value of the Darcy number are not so strong.

Therefore, the minor changes appearing between the results of different Darcy numbers are expected. Figure 14 indicates that with increase in the Darcy number, the flow needs more distance to become thermally developed.

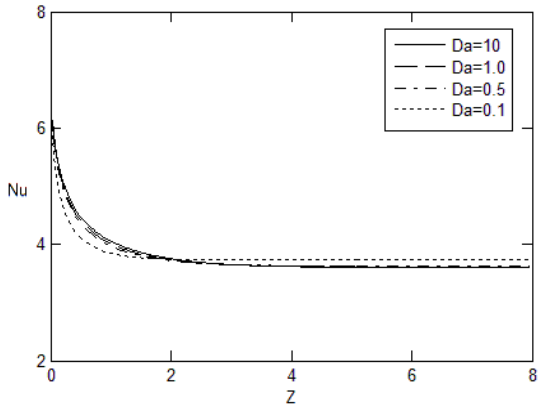

Fig. 14. Effect of the Darcy number on the distribution of the local Nusselt number through the micro-tube ($Kn = 0.1, Pe = 100, \Gamma = 10, Bi = 1, K_R = 1$)

Figure 15 serves as a companion to this figure. The figure illustrates the variations of the thermal entry length with the Darcy number for different cases of the gas rarefaction in the slip flow regime. Effect of the Darcy number on the thermal entry length is obvious in $0.01 \leq Da \leq 1$. With further increase in Da, however, the changes appearing in the thermal entry length are not so substantial. This occurs since in higher values of the Darcy number, the consequences of the frictional resistance of the medium vanish and the flow in the porous medium tends to the flow in a clear domain. Figure 14 also demonstrates that with increase in the Knudsen number, at a constant Darcy number, it takes longer distance for the flow to become thermally developed. This is in accord with our previous observation in Figure 13.

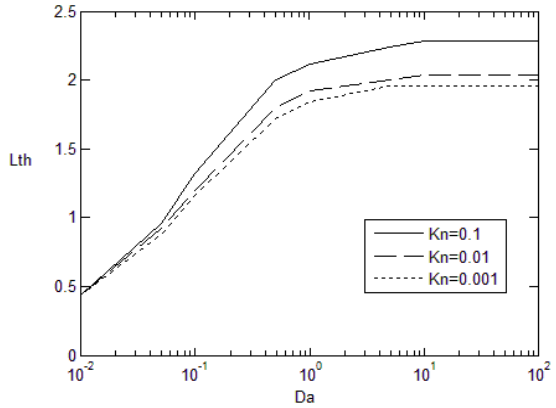

Fig. 15. Effect of the Darcy number on the thermal entry length ($Pe = 100, \Gamma = 10, Bi = 1, K_R = 1$)

Figure 16 shows the effect of the Forchheimer number on the distribution of the local Nusselt number through the micro-tube. Similar to the Darcy number, notice that the Forchheimer number does not produce similar consequences in the developing and the developed regions of the tube. Indeed, any increase in the Forchheimer number (i.e., increase in the inertial resistance of the medium) leads to decrease in both velocity slip and temperature jump at the wall. Here, the diminished velocity slip tends to reduce the Nusselt number while the decreased temperature jump produces an opposite effect. In the developing region, the diminished velocity slip is dominant causing heat transfer reduction as a result of increase in the Forchheimer number. Conversely, when the gas becomes thermally developed, the decreased temperature jump overcomes the effect of the diminished velocity slip. This produces heat transfer improvement as a result of increase in the Forchheimer number there. The minor consequences are, however, expected since the variations of the wall velocity slip and temperature jump with the Forchheimer number are not so strong.

Inspection of Figure 16 indicates that with increase in the Forchheimer number, the flow becomes thermally developed more quickly. To demonstrate this effect further, variations of the thermal entry length with the Forchheimer number for different Knudsen numbers are plotted in Figure 17.

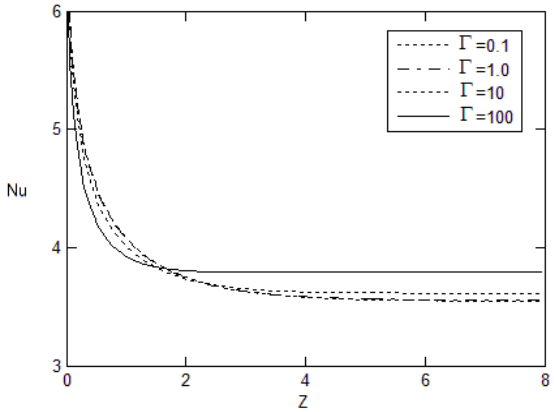

Fig. 16. Effect of the Forchheimer number on the distribution of the local Nusselt number through the micro-tube ($Kn = 0.1, Pe = 100, Da = 1, Bi = 1, K_R = 1$)

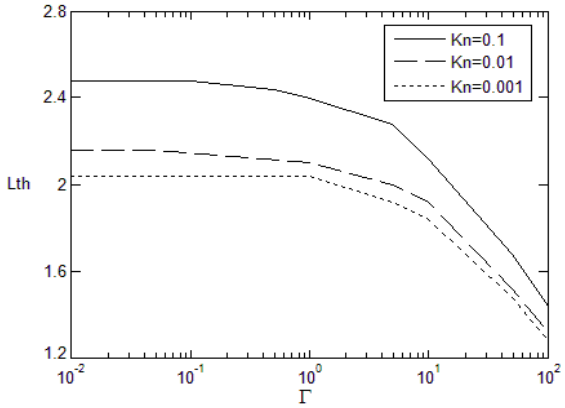

Fig. 17. Effect of the Forchheimer number on the thermal entry length ($Pe = 100, Da = 1, Bi = 1, K_R = 1$)

The figure demonstrates that for $\Gamma \geq 1$, any increase in the Forchheimer number reduces the thermal entry length.

For $\Gamma < 1$, however, notice that this parameter is not so influential. It is also obvious that the role of the Knudsen number on the thermal entry length is more significant at lower values of Γ since velocities are relatively high there.

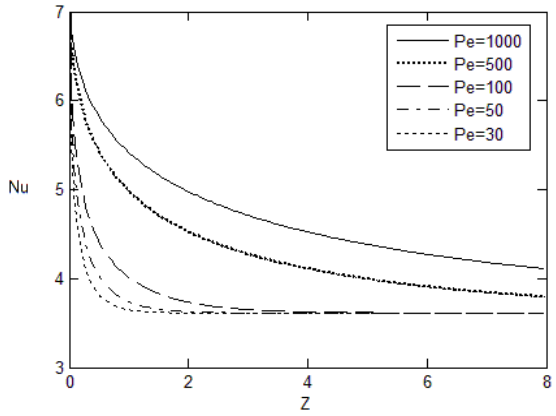

Fig. 18. Effect of the Peclet number on the distribution of the local Nusselt number through the micro-tube ($Kn = 0.1, \Gamma = 10, Da = 1, Bi = 1, K_R = 1$)

In Figure 18, the effect of the Peclet number on the distribution of the local Nusselt number is illustrated. Notice the heat transfer improvement as a consequence of the increase in the Peclet number. This goes back to the increased gas flow velocities in the forced convection regime. The figure also indicates that the flow in higher Peclets requires longer distance to become thermally developed. This behavior is provided in a better picture in Figure 19. The figure demonstrates that the Peclet number is more influential at higher rarefactions.

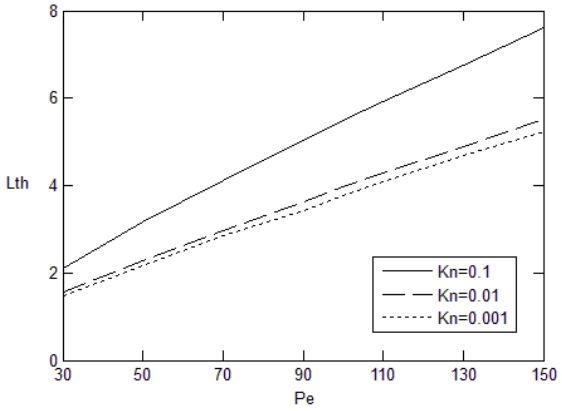

Fig. 19. Effect of the Peclet number on the thermal entry length ($Kn = 0.1, \Gamma = 10, Da = 1, Bi = 1, K_R = 1$)

Figure 20 shows the effect of the Biot number on the distribution of the local Nusselt number through the micro-tube. Since increase in the Biot number improves the heat exchange between the fluid and the porous matrix, the appeared heat transfer enhancement as a result of increase in the Biot number is expected. The figure also illustrates that with change in the Biot number, the thermal entry length remains almost constant.

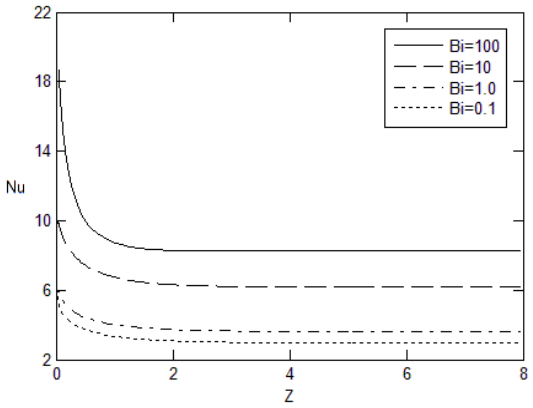

Fig. 20. Effect of the Biot number on the distribution of the local Nusselt number through the micro-tube ($Kn = 0.1, Pe = 100, \Gamma = 10, Da = 1, K_R = 1$)

Finally, the effect of the modified conductivity ratio on the distribution of the local Nusselt number is given in Figure 21. Heat transfer reduction as a result of increase in $K_R$is obvious. This occurs as a consequence of decrease in thermal conduction in the solid matrix that deteriorates the heat transfer from the tube wall to the porous matrix and then, from the porous matrix to the gas flow. Notice also that the thermal entry length is not so sensitive to the value of K_R.

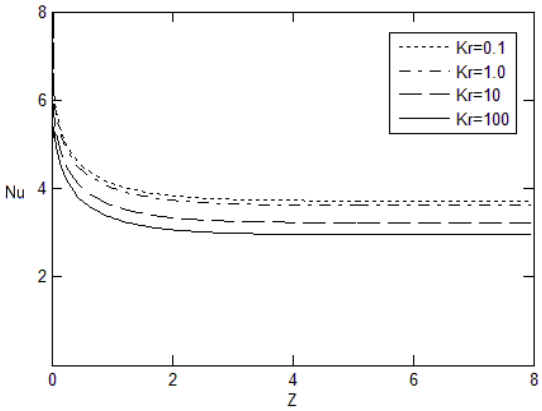

Fig. 21. Effect of the modified thermal conductivity ratio on the distribution of the local Nusselt number through the micro-tube ($Kn = 0.1, Pe = 100, \Gamma = 10, Da = 1, Bi = 1$)

CONCLUDING REMARKS

Forced convection heat transfer of slip flow in porous micro-tubes was investigated here numerically. Key observations are summarized as follows:

1. Increase in the Peclet/Biot number improves the heat transfer performance while increase in the Knudsen number or the modified conductivity ratio diminishes it

2. Effects of the Darcy/Forchheimer number on the heat transfer performance are not similar in the developing and the developed regions of the flow
3. With increase in the Knudsen number, the Peclet number, and the Darcy number or decrease in the Forchheimer number, the flow needs longer distance to become thermally developed. Thermal entry length is not, however, so sensitive to the Biot number and the modified conductivity ratio.

REFERENCES

[1] Schaaf SA, Chambre PL. Flow of Rarefied Gases: Princeton University Press, Princeton, 1961.

[2] Gad–el–Hak M.The fluid mechanics of microdevices the freeman scholar lecture. ASME Journal of Fluids Engineering. 1999;121:5–33.

[3] Zahmatkesh I, Alishahi MM, Emdad H.New velocity –slip and temperature–jump boundary conditions for Navier-Stokes computation of gas mixture flows in microgeometries. Mechanics Research Communications. 2011;38:417–424.

[4] Zahmatkesh I, Emdad H, Alishahi MM.Navier Stokes computation of some gas mixture problems in the slip flow regime. Scientia Iranica B. 2015;22(1):187–195.

[5] Haddad OM, Al–Nimr MA,Taamneh Y.Hyrodynamic and thermal behavior of gas flow in microchannels filled with porous media. Journal of Porous Media. 2006;9:403–414.

[6] Haddad OM, Al–Nimr MA, Sari MS.Forced convection gaseous slip flow in circular porous micro–channels. Transport in Porous Media. 2007;70:167–179.

[7] Haddad OM, Al–Nimr MA, Al–Omary JSh. Forced convection of gaseous slip–flow in porous micro–channels under local thermal non–equilibrium conditions. Transport in Porous Media. 2007;67: 453–471.

[8] Shokouhmand H, Isfahani AHM, Shirani E. Friction and heat transfer coefficient in micro and nano channels filled with porous media for wide range of Knudsen number. International Communications in Heat and Mass Transfer. 2010;37:890–894.

[9] Neild DA, Kuznetsov AV. Forced convection with slip flow in a channel or duct occupied by hyper–porous medium saturated by rarefied gas. Transport in Porous Media. 2006;64:161–170.

[10] Hooman K. Heat and fluid flow in rectangular microchannel filled with a porous medium. International Journal of Heat and Mass Transfer. 2008;51:5804–5810.

[11] Mahmoudi Y. Constant wall heat flux boundary condition in micro–channels filled with porous medium with internal heat generation under local thermal non–equilibrium condition. International Journal of Heat and Mass Transfer. 2015;85:524–542.

[12] Buonomo B, Manca O, Lauriat G. Forced convection in micro–channels filled with porous media in local thermal non–equilibrium conditions. International Journal of Heat and Mass Transfer. 2014;77:206–222.

[13] Buonomo B, Manca O, Lauriat G. Forced convection in porous microchannels with viscous dissipation in local thermal non–equilibrium conditions. International Communications in Heat and Mass Transfer. 2016;76:46–54.

[14] Wang K, Tavakkoli F, Wang S, Vafai K. Forced convection gaseous slip flow in a porous circular microtube: An exact solution. International Journal of Thermal Sciences. 2015;97:152–162.

[15] Torabi M, Peterson GP. Effect of velocity slip and temperature jump on the heat transfer and entropy generation in micro porous channels under magnetic field. International Journal of Heat and Mass Transfer. 2016;102:585–595.

[16] Neild D, Bejan A. Convection in Porous Media: Springer, New York, 2013.

[17] Karniadakis G, Beskok A, Aluru N. Microflows and Nanoflows: Fundamentals and Simulation: Springer, New York, 2005.